Brief communication: Sensitivity analysis of peak water to ice thickness and temperature: A case study in the Western Kunlun Mountains of the Tibetan Plateau

Lucille Gimenes[1], Romain Millan[1], Nicolas Champollion[1], and Jordi Bolibar[1]

[1]Univ. Grenoble Alpes, CNRS, IRD, G-INP, Institut des Géosciences de l'Environnement, Grenoble, France

Correspondence: Lucille Gimenes (lucille.gimenes@univ-grenoble-alpes.fr) and Romain Millan (romain.millan@univ-grenoble-alpes.fr)

Abstract. This study investigates the sensitivity of peak water in the western Kunlun Mountains of the Tibetan Plateau. Using the Open Global Glacier Model (OGGM), we analyze how variations in inverted initial ice volume and temperature bias under different ~~climate scenarios~~ Shared Socioeconomic Pathways (SSP) affect peak water timing and magnitude. We compare two global ice thickness datasets, revealing substantial differences in the ~~predicted~~ projected peak water timing and magnitude. The results highlight that smaller initial ice volumes lead to earlier peak water occurrences, particularly under the SSP5-8.5 scenario. Temperature bias also ~~significantly influences runoff magnitude and the timing of peak water , especially under high-emission scenarios~~notably influences the peak water timing by delaying its date in the region by roughly 13 years for each bias degree. These findings underscore the importance of accurate ice thickness estimates and climate projections for predicting future water availability and informing water management strategies in glacier-dependent regions.

1 Introduction

Modeling the future evolution of glaciers is essential due to their significant impact on sea level rise (0.61 ± 0.08 mm Sea Level Equivalent - SLE - yr^{-1} for the 2006-2015 period) and freshwater resources ~~(Nauels et al., 2017)~~(Hock et al., 2019a) . Consequently, the projected changes in runoff will ~~also~~ impact downstream water management (Hock et al., 2019b). With increasing air temperatures, glacier ablation and therefore glacier runoff is expected to rise and reach a maximum (if it is not already reached as it is the case in many regions), defined as "peak-water," after which glacial freshwater outputs will decline due to the shrinking glacier area (Huss and Hock, 2018). Determining ~~precisely the~~ the precise timing and magnitude of maximum runoff is therefore of prime importance for freshwater management, likely affecting ecosystems, drinking water resources as well as other sectors such as agriculture or hydro-power production (Arias et al., 2021).

~~The indirect inversion of ice thicknesses is a critical step which can have a substantial impact on the peak water (Huss and Farinotti, 2012) . However, existing glacier thickness estimations are uncertain and exhibit notable differences in both the spatial distribution and the overall volume of glaciers (Farinotti et al., 2019; Millan et al., 2022). Advances~~ However, projections of glacier runoff remain uncertain due to biases in both climate forcing and initial glacier geometry, the latter depending on ice thickness estimates (Huss and Hock, 2015). Inversion of ice thicknesses is a major source of uncertainty, influencing modeled ice volumes

and consquently the timing of peak water (Huss and Farinotti, 2012). Recent advances in satellite remote sensing have ~~allowed the emergence of new global data products~~produced new global datasets, such as ~~the first global estimate~~ ice thickness maps derived from surface flow velocities (Millan et al., 2022) and global estimates of glacier mass change (Hugonnet et al., 2021)~~or global mapping of thicknesses based on surface flow velocities (Millan et al., 2022). Among available large-scale glacier models, flowline models like the Open Global Glacier Model (OGGM, Maussion et al., 2019) or the Global Glacier Evolution Model (GloGEM, Huss and Hock, 2015) are based on flowline versions of the Shallow Ice Approximation (SIA, Hutter, 1983). On the other hand, models such as Elmer/Ice (Gagliardini et al., 2013) or the Ice Sheet System Model (ISSM, Larour et al., 2012) work in three dimensions with a higher degree of complexity, especially concerning ice dynamics, and numerous parameters to optimize (Zekollari et al., 2022). Simulations are therefore more computationally expensive, and more challenging to apply on a large scale. The very recent development of emulators based on deep learning, or the implementation of universal differential equations, holds strong potential to address these issues to better simulate glacier flow dynamics (Jouvet, 2023; Bolibar et al., 2023) but not yet applicable at large scale. Therefore, despite the limitations of global scale models (essentially flowline and approximation of ice dynamics), the growing developments and physics improvements, along with their user-friendly nature, make them unique and useful tools for estimating the evolution of all worldwide glaciers (Marzeion et al., 2018; Rounce et al., 2023; Zekollari et al., 20~~
. Yet large discrepancies persist between these datasets, particularly in High Mountain Asia, where total ice volume estimates differ by up to 35% between products (Farinotti et al., 2019; Millan et al., 2022).

The Western Kunlun Mountains are located at the northern edge of the Tibetan Plateau. This is a major glacierized region within the Tarim Interior River Basin (TIRB), where glacial meltwater contributes to downstream water resources (Immerzeel et al., 2020). Despite its importance, this region is subject to the largest discrepancies among existing ice thickness datasets, making it an ideal case to illustrate how geometry uncertainty influences modeled glacier runoff. While several studies have investigated the estimation of peak water at regional and global scales (Huss and Hock, 2018; Caro et al., 2025), there are to date, few quantitative assessments of how uncertainties in initial glacier geometry and climate model biases influence its timing and magnitude.

In this study, we ~~investigate the sensitivity of peak water~~ examine how uncertainties in ice thickness estimates and temperature affect the timing, magnitude~~and duration, to different inverted ice volumes and temperature bias.~~, and duration of peak water in a region with strong variability between existing datasets and strong vulnerability to climate change in terms of water supply (Immerzeel et al., 2020): the Western Kunlun Mountains on the Tibetan Plateau. We first propose a methodology to assimilate ice thickness inversions into the OGGM model, with an approach that can be applied globally. We then perform sensitivity experiments by perturbing both initial ice volume and climate forcing to quantify their combined effects on peak water. Finally, we illustrate the role of glacier geometry by comparing two widely used ice thickness datasets that differ substantially in this region.

2 Data and Methods

2.1 Region of interest

Our study focuses on the northern part of the Karakoram, more precisely within the West Kunlun mountain range, situated at the confluence of the Xinjiang Autonomous Region and the Tibetan Plateau~~(RGI Consortium, 2017)~~. This study specifically targets a group of 160 glaciers with a total surface area of approximately 2900 km^2, calculated with the RGI v6 (RGI Consortium, 2017) (Fig. 1)~~. These~~, which was used in the two ice thickness datasets that are being evaluated in this study. The glaciers are located at very high elevations (5500-6400 m, Ke et al., 2015) ~~,~~ in a region characterized by largely sub-zero temperatures, often reaching -10°C on annual averages. This region has an icefield-like geometry that is hosting a large variety of glaciers. The northern part of the selected region has a steeper terrain, with mostly valley glaciers, while the southern region has a less marked relief with glacial features close to the geometry of an ice cap (Ke et al., 2015). Surface flow velocities derived from radar measurements spanning from 2003 to 2011 reveal that nearly 70% of the largest glaciers in the region exhibit a normal flow type, characterized by a continuous downstream flow. Additionally, 10% of ~~these~~ glaciers are identified as surging glaciers, while the remaining 20% display nearly stagnant velocity profiles (Yasuda and Furuya, 2013).

In terms of mass balance, West Kunlun is ~~,~~ within the region of High Mountain Asia ~~,~~ affected by what is called the "Karakoram anomaly": in 2000-2016, glacier mean elevation change (0.26 ± 0.07 m w e yr^{-1}) and region-wide mass balance (0.14 ± 0.08 m w e yr^{-1}) ~~was~~ were mostly positive (Brun et al., 2017). However, during the 2000-2019 period ~~,~~ Hugonnet et al. (2021) found a regional mean elevation change rate of ~~-9.6~~ -0.23 ± 0.04 m yr^{-1} for the Central Asia region (RGI region 13, RGI Consortium, 2017), where West Kunlun is located, indicating an overall downward trend. Specifically, their findings highlight a shift towards thinning ~~,~~ particularly notable in the late 2010s, signifying a potential conclusion to the previously observed Karakoram anomaly.

Furthermore, the glaciers within the scope of this study are situated in the ~~Tarim Interior River Basin (TIRB),~~ TIRB as indicated by the green shading in Fig. 1a (Lehner et al., 2008). Specifically, the Kunlun mountain range serves as a primary water source for the Tarim River, a key component of the TIRB, which flows across the Tarim desert (Gao et al., 2010). According to Immerzeel et al. (2020), the water tower unit of Tarim Interior is defined as the overlap between the Tarim Interior hydrological basin from Lehner et al. (2008) and various mountain ranges from Körner et al. (2017) within the basin. This unit plays a pivotal role in providing water to ecosystems and the downstream population. Tarim is recognized by Immerzeel et al. (2020) as one of the most significant water units in Asia, with a notably high contribution of glacier water yield compared to precipitation in the basin. Despite this, the downstream supply often struggles to meet the increasing water demand driven by industrial, domestic, and primarily irrigation needs in the case of TIRB (Immerzeel et al., 2020). Consequently ~~,~~ this basin stands out as one of the most vulnerable, susceptible to the impacts of climate, political, and socioeconomic changes ~~. However, a~~ (Immerzeel et al., 2020). A study focusing on glacier runoff changes using GloGEM (Huss and Hock, 2018) already anticipates a rise in Tarim's annual glacier runoff until around 2050, followed by a consistent decline for the remainder of the 21st century under the RCP4.5 emission scenario.

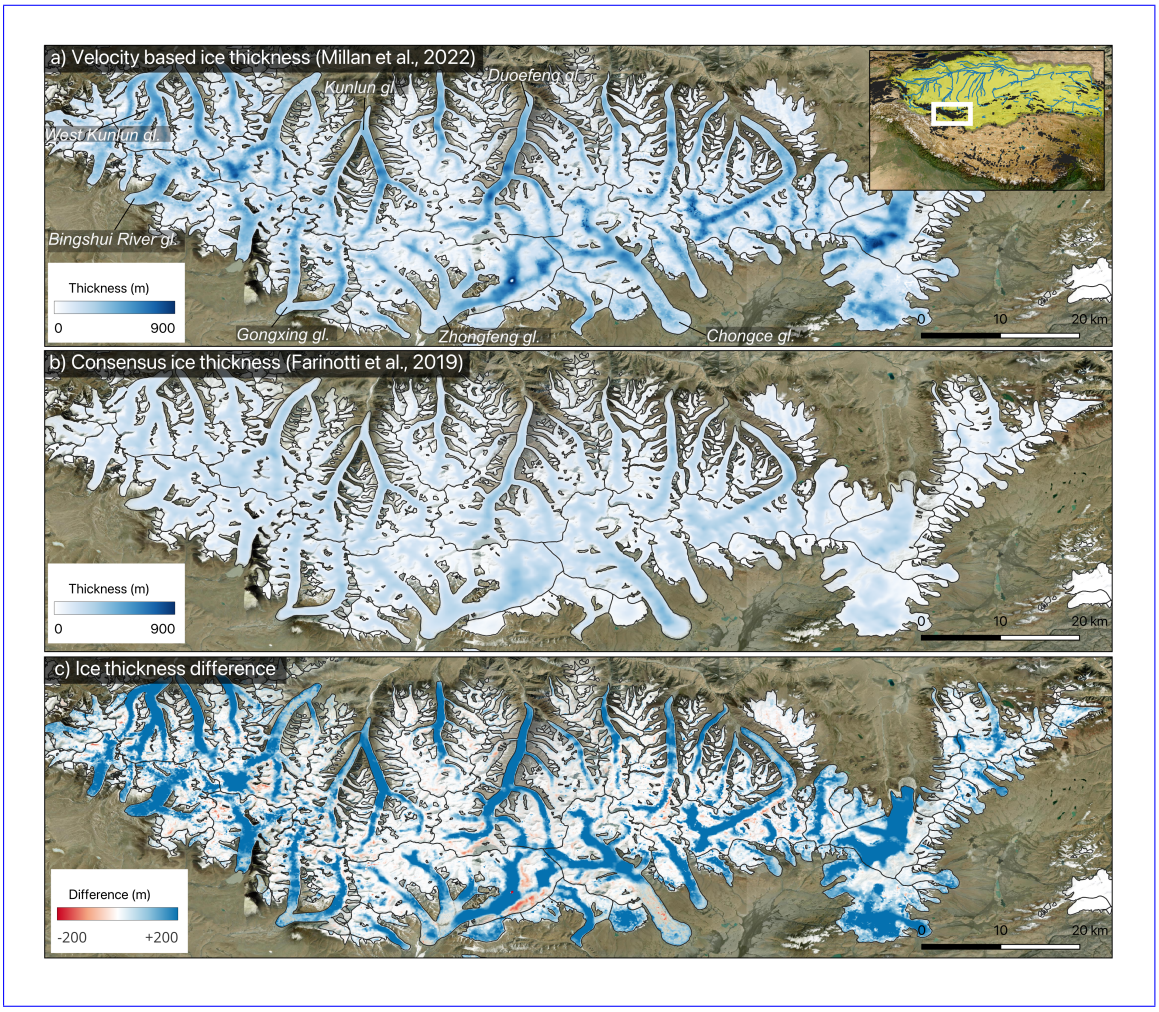

Figure 1. Map of the study region: (a) ice thickness from Millan et al. (2022) (with the location of the study set in the Himalayan area); (b) ice thickness from Farinotti et al. (2019); and (c) difference between (a) and ~~ice thickness from Farinotti et al. (2019)~~(b). Glacier boundaries are from the ~~Randolph Glacier Inventory~~ RGI v6 (RGI Consortium, 2017). Basemap is a mosaic of images from Copernicus Sentinel-2 data generated via sentinel-hub (Sinergise Solutions d.o.o.). Green area on the insert map corresponds to the Tarim Interior River Basin.

2.2 Ice thickness dataset

In this study, we will compare the timing and magnitude of the peak water ~~predicted~~ simulated using two existing global ice thickness datasets. The first is the consensus ~~for~~ obtained in 2019 (abbreviated FARI19, Fig. 1b, Farinotti et al., 2019), which provides a global estimate (except for the Greenland and Antarctic ice sheets) of ice volumes for individual glaciers ~~with the help of~~ using five different models ~~,~~ selected from the Ice Thickness Inter-comparison Project (ITMIX, Farinotti et al., 2017). Inversion methods are based on the use of the principle of mass conservation (Huss and Farinotti, 2012; Maussion et al.,

2019), empirical relationships between basal shear stress and glacier elevation change (Linsbauer et al., 2012), or the use of flux thickness inversion (Fürst et al., 2017). One ~~of the common approach in between~~ common approach among these models (excepted for Fürst et al., 2017) is the use of flowline inversions "glacier by glacier~~flowline inversions~~ ", based on elevation data from Digital Elevation Models (DEMs). The second ice thickness model used in this study (abbreviated MIL22, Fig. 1a, Millan et al., 2022) is based on the inversion using jointly surface ice flow velocity and surface slopes. This inversion makes use of a new global ice velocity product, that provides measurements for 98% of the world's glaciers in the years 2017-2018, at a sampling resolution of 50 meters. Inversions are also based on the ~~SIA~~Shallow Ice Approximation (SIA) (Hutter, 1983) , but are performed regionally and in two dimensions. This approach revealed a different picture of the distribution of ice thicknesses and the ice volume of some regions around the Earth (Millan et al., 2022; Hock et al., 2023; Frank and van Pelt, 2024)~~. Specifically, the Asia region (RGI 13/14/15) displayed a significant difference from the consensus estimate, with total glacier ice volume around 35% higher than the consensus over the same surface area (Farinotti et al., 2019; Millan et al., 2022)~~ , with notable differences specifically in the RGI region of this study. The Himalayan region is indeed one of the most uncertain in terms of ice thickness inversion, with very few direct measurements available to constrain the physical parameters of the inversion~~(e.g., fewer than 10 glaciers were available to calibrate the results of Millan et al., 2022).~~ . Fewer than 10 glaciers were available to calibrate the results of Millan et al. (2022), and Farinotti et al. (2019) used thickness measurements from the Glacier Thickness Database (GlaThiDa) v2 (WGMS, 2016), with less than 50 glaciers being covered within this RGI region.

In this paper, we ~~are specifically interested in differences over~~ focus on differences within a sub-region of the West Kunlun ~~mountain. Since the~~ Mountains. The consensus model is ~~dated from 2003, and that Millan et al. (2022) uses ice velocity centered in the year 2017-2018~~approximately dated to 2000: the selected glaciers' RGI outlines are from 2010, but FARI19 used the 2000–2001 SRTM DEM for thickness inversions in this region. Since Millan et al. (2022) relies on ice velocities centered on 2017–2018, we corrected the MIL22 estimates ~~using average glacier mass changes~~ to obtain thicknesses corresponding to the year 2000. As correction, we simply subtracted average glacier thickness changes of Hugonnet et al. (2021) between 2000 and ~~2020~~ 2019, which is obtained from DEM differencing~~(Hugonnet et al., 2021)~~, to MIL22 thicknesses. While solving temporal ambiguities of the thickness models is complicated, since DEM sources and in-situ data are not properly dated, this correction may be a step toward roughly matching the timing of the consensus estimate. Overall, differences after ~~correcting from~~ correction for glacier mass change ~~averages 4.0~~ average 6 km^3 ~~from~~ compared to the original MIL22 estimate, representing 1 % of the latter. Finally, the ~~total~~ ice volume totals ~~344~~ 345 km^3 and ~~562~~ 570 km^3 for FARI19 and corrected MIL22 respectively (Fig. 1c). It is worth noting that ice thickness is in general, systematically higher for MIL22 than for Farinotti, both at low and high elevations (Fig 1c), with differences reaching up to 200 meters along glacier trunk.

2.3 ~~Description of the glacier model~~

2.3 Open Global Glacier Model (OGGM) - v1.6

~~The Open Global Glacier Model version 1.5 used here is an~~ OGGM is an open-source ~~model that aims to simulate the past and future evolution of glaciers on regional to global scales (). The model starts by using the outlines from the RGI~~

(RGI Consortium, 2017) and project them onto a local grid whose resolution depends on glacier size. Topographical data are also added to the grid which sources depends on the glacier location and are part of the glacier evolution model that uses RGI outlines (RGI Consortium, 2017) and topographical data from various sources (NASADEM, COPDEM, GIMP, TANDEM or MAPZEN . The model computes centerlines with the help of a geometrical routing algorithm (Kienholz et al., 2014) that optimizes the path between local elevation maxima and the glacier 's terminus in order to minimize total elevation gain and distance to the glacier terminus. These centerlines are modified into proper flowlines , with grid points evenly distributed according to a spacing dependent on the grid resolution, and whose elevation is determined from the topography grid. It is worth mentioning that a flowline downstream of the current glacier extent (i.e such as defined by the RGI) is also computed, so that it could possibly grow. For every flowline, a catchment area is determined and used to elaborate depending on the glacier location) to compute flowlines made of evenly distributed grid points, which are assigned geometrical cross-sections at each point, by intersecting the normal to the flowline with the glacier outlines or the catchment areas. These cross-sections are then corrected in respect to the altitude-area distribution of the glacier (Maussion et al., 2019).

After determining these geometrical parameters, OGGM computes the glacier mass balance for each cross-sections, Surface mass balance is calculated for each cross section according to a temperature-index model with a single temperature sensitivity factor for the entire glacier (Marzeion et al., 2012; Maussion et al., 2019). The monthly surface mass balance is calculated as a the sum of accumulation and ablation on the glacier, which are functions of temperatures a function of air temperature and precipitation. For this purpose, we used OGGM retrieves gridded climate data, which is by default the latest monthly time series from the Climate Research Unit (CRU, Harris et al., 2020), but also other climate data sources such as ERA5 (Hersbach et al., 2019) from the European Centre for Medium-Range Weather Forecasts (ECMWF) or climate projections from the Coupled Model Intercomparison Project CMIP5 (Taylor et al., 2012) and CMIP6 (Eyring et al., 2016) for future projections. that can be observational time series for historical runs as well as climate projections for future simulations. The surface mass balance model is calibrated on geodetic mass balance observations obtained from remote sensing (Hugonnet et al., 2021) for the 2000-2019 time period, using the W5E5v2.0 climate dataset as forcing (Lange et al., 2021). With these surface mass balance estimates as input, OGGM uses a flux-based ice flow model to solve a mass conservation equation along flowlines, under the SIA hypothesis, deriving ice thickness at each cross section. We also make use of a feature from the latest version of OGGM which is a dynamic spin-up that can provide glacier initial state for the year 2020 by reconstructing its recent past while ensuring that modeled glacier area and observed one are matched within 1 % at the inventory date under historical climate forcing (Aguayo et al., 2023; Zekollari et al., 2024). Finally, the model gives as simulation outputs glacier volume, length and area, as well as glacier runoff. Considering a fixed glacier area including glacierized and increasingly non-glacierized terrain, the annual total runoff computed in OGGM is derived as the sum of snow melt on now ice-free area, the ice and seasonal snow melt on glacier, the liquid precipitation on glacier, and the liquid precipitation on now ice-free area (e.g. in Fig. S1).

Finally, OGGM calibrates parameters of the Surface Mass Balance (SMB) model (such as temperature sensitivity or precipitation factor) with the help of SMB observations from the World Glacier Monitoring Service WGMS (2021). In the latest model version , OGGM employs global remote sensing data and a new calibration scheme based on global glacier volume changes (Hugonnet et al., 2021). However, this study is based on an earlier calibration framework as described in Maussion et al. (2019)

, which was the most recent version at the time of the analysis. Because we are performing a sensitivity analysis focused on the role of glacier ice thickness — and all simulations use the same climate forcing and calibrated mass balance parameters — the relative differences in runoff evolution are driven primarily by the initial geometry rather than the specific calibration. This is consistent with previous studies (Maussion et al., 2019; Huss and Hock, 2015), which emphasize the importance of initial glacier geometry — particularly ice thickness — as a key source of uncertainty in glacier evolution modeling. Thus, the fact that we do not use the updated calibration based on Hugonnet et al. (2021) observations implies that our experiments reflect an average sensitivity of peak water to initial conditions across the region. Implementing the new calibration methods now

2.4 Climate forcing

To compute monthly glacier surface mass balance, we use monthly temperature and precipitation time series as forcings. The W5E5 dataset (spatial resolution of 0.5°) is used by OGGM as standard baseline climate for dynamical spin-up or historical runs on the 1979-2019 time period. In order to perform projection runs extending from 2020 until 2300, we use General Circulation Models (GCM) climate data with resolution ranging from 1.12° to 2.5° originating from the Coupled Model Intercomparison Project CMIP6 (Eyring et al., 2016), which employs Shared Socioeconomic Pathways (SSP) as scenario framework (Riahi et al., 2017). Out of the 6 different GCMs extending until 2300 available in OGGMwould allow a closer match to observed mass balance values and consequently more accurate estimates of real peak water timing and magnitude. However, this is not the aim of the present study that focuses on exploring the sensitivity of peak water timing and magnitude to uncertainties in glacier ice thickness, particularly in a regionwhere discrepancies between inversion methods are substantial.

The model then makes use of the computed surface mass balance to estimate the ice thickness for each cross section. To that aim, OGGM inversion method starts from the mass conservation equation and SIA hypothesis applied to the flowline geometry in order to derive ice thickness at each cross section as a function of , this study is carried out with 5 of them : MRI-ESM2-0, CESM2-WACCM, IPSL-CM6A-LR, ACCESS-CM2 , and ACCESS-ESM1-5. CanESM5 is omitted on the bedrock shape (rectangular, trapezoidal or parabolic cross section) and grounds of providing an unrealistic temperature increase in the region. The reanalysis data from 2000-2019 is used as reference climatology for bias correction of the 5 GCMs, following the anomaly method implemented in OGGM. Simulations are conducted with the "apparentr1i1p1f1"surface mass balance (equilibrium assumption of the glacier geometry, Maussion et al., 2019), from which will result the computation of the whole glacier ice thickness and bedrock, used to finally calculate glacier volume, length and area. OGGM uses a dynamical ice flowline forward model to simulate the evolution of the glacier geometry in response to the SMB forcing, resulting itself from any given climate observations or projections. -tagged ensemble member for each GCM under three different pathways: SSP1-2.6, SSP5-3.4-Overshoot (OS) (only 3 of the GCMs are forced under this scenario) and SSP5-8.5. It must be acknowledged that SSP5-3.4-OS is actually not an intermediate scenario since it explores the implications of a peak and decline in forcing during the 21st century (Lee et al., 2021). The choice to use a rather small number of GCMs would be inaccurate if we were trying to assess accurately and precisely the future evolution of glaciers, but here we are solely interested in the study of the impact of different ice thickness datasets on glacier evolution and their runoff.

2.5 Integration of ice thickness datasets into OGGM

~~Due to the fact that Open Global Glacier Model (OGGM)~~ Since OGGM is based on a flowline representation of glacier geometry, limitations can be found when incorporating large two dimensional datasets from remote sensing observations. Consequently, the assimilation of such thickness models into OGGM is not a trivial question. In this paper ~~,~~ we have chosen to investigate the influence of the total ice volume on the glacier contribution to runoff, hence we do not explore spatial and 2D differences between ice ~~thicknesses~~ thickness models. To integrate ice thickness datasets in OGGM, we first calculate ~~, from satellite or model-based observation,~~ from observations the total ice volume for each glacier entity in the region of interest. Secondly, we invert ice thicknesses within the model framework (section 2.3). Finally, the creep parameter A - that describes ice deformation - is calibrated ~~,~~ in order to reach the total volume calculated with the observed datasets. If the model cannot converge ~~toward~~ on a consistent value of the creep parameter, ~~it will add~~ a non-zero sliding parameter f_s ~~(that is normally set as zero for all glaciers, Maussion et al., 2019)~~is added, taking into account that it is normally set to zero for all glaciers (Maussion et al., 2019). This approach avoids model instabilities that can be found during spin-up processes, with the direct integration of ice thickness ~~dataset~~ datasets in OGGM. Indeed, the latter could potentially disrupt the whole glacier ~~dynamic~~dynamics, since the observed ice thicknesses ~~are not~~ might not be consistent with its modeled volume or its DEM, for example, which could lead to ~~the glacier rebalancing itself~~ a numerical shock at the beginning of ~~each simulations~~the simulation.

After ~~the calibration of the OGGM~~ performing the ice thickness inversions, we find a difference of 0.3 % $\pm$ 4.5 % with the volume derived from the ice thickness data calculated from Millan et al. (2022) and Farinotti et al. (2019). This is negligible compared to the difference between the two ice thickness datasets which is roughly 40% (Millan et al., 2022; Farinotti et al., 2019) in the study region. ~~After this assimilation process of~~ Once the ice thicknesses assimilation process is done, ~~the glacier initial state is ready to be used for different types of simulations.~~

~~In this study, we did not used any spin up procedure because of the large uncertainties in climatic data in Asia. The West Kunlun region is one of the least covered areas by weather stations in Asia, resulting in significant spatial uncertainties in temperature and precipitation data Wester et al. (2019). Hence the climate data used for the~~ glaciers are initialized for the year 2020 by running the OGGM dynamic spin-up ~~procedure are mostly the results of large interpolations. These interpolations resulted in erroneous positive temperature bias, which reduced the ice volume close to zero for the Farinotti dataset during one of the spin-up tests~~starting in 2000, setting up the initial conditions to be used for this study's simulations.

2.6 Peak water calculation

We ~~calculate~~ assess the impact of initial ice thickness on ~~the glacier hydrological mass-balance~~ glacier hydrological surface mass balance outputs, and more specifically on the timing and magnitude of the peak water. ~~Considering a fixed glacier area, including glacierized and increasingly non-glacierized terrain, we first derive the annual total~~ After performing simulations for all glaciers with different ice thicknesses, we consider the sum of all their annual runoff as the ~~sum of (1) snow melt on now~~

ice-free area, (2) the ice and seasonal snow melt on glacier, (3) the liquid precipitation on glacier and (4) the liquid precipitation on now ice-free area (Fig. S1). All these variables are outputs of the OGGM model.

regional annual runoff, which is then averaged over a 10-year window in order to smooth inter-annual variability and highlight long-term trends. While the principle of peak water is often presented as a single maximum value (Huss and Hock, 2015), our simulations often reaches a maximum peak water reach a maximum regional runoff "plateau", which remain remains constant for several years or decades. In order to To measure the extent of this plateau, we empirically chose to use runoff values included in the top decile. Then, to rule out define it as the top 10 % of simulated runoff values for SSP5-8.5 (and as the top 5 % for other SSPs). To pick one single date value for peak water timing, we selected the median runoff date along the plateaudate of the plateau's temporal extent. Similarly for the associated quantity of water runoff, we use the average of the annual runoff on the plateau. After performing simulations on all glaciers with different thicknesses, we consider the sum of all their annual runoff as the region annual runoff, which is averaged over a 10-years window. plateau's values.

It is worth noting that, starting from glacier equilibrium and considering climate warming "enough " higha climate that has warmed enough to cause substantial glacier retreat, peak water is thus defined as a tipping point where glacier area has shrunk sufficiently that any further climate evolution can't result in this maximum represents the tipping point beyond which any additional warming leads to a decline in glacier contribution to basin runoff (Huss and Hock, 2015). In other wordwords, considering a moderate climate warming followed by a temperature decrease, we can reach a temporary maximum of glacier runoff that looks like an "apparent" peak water which but is not a tipping point. In order to To additionally investigate the initial ice volume influence on peak water, we design an ensemble of simulations with different values of total ice thickness of all selected glaciers, by multiplying the initial inverted volume from Millan et al. (2022) of the entire glacier by multiplying this volume (using MIL22 initial ice thicknesses, see section 2.5) by a coefficient ranging from 0.1 to 2 for each individual glacier of the study set . We simulate their evolution using climate data from CRU for historical runs and the GCM MRI-ESM2-0 for all glaciers. We do not use the dynamical spin-up in this set up since it can not converge to match the RGI area with the amount of simulated reduced or increased ice volume. Instead, after ice thicknesses assimilation we simulate glaciers evolution from 2000 to 2020 simply using historical W5E5 data to initialize glaciers before future projections (see section 2.4). Similarly, we examined examine the influence of temperatures on the air temperature on peak water. To this aim, we simulate the evolution of glaciers with conceive an ensemble of projection runs (using also using the MIL22 initial ice thicknesses, see section 2.5) by adding temperature biases dataset) adding a uniform temperature bias (ranging from -5 to 5°C) over the full simulation period, meaning that a this bias is added to the temperatures air temperature time series used by the model to calculate surface mass balance (see section 2.3).

2.7 Climate data

In order to compute monthly glacier mass balance , we use monthly temperature and precipitation time series as forcings. The simulations include first historical runs, using observational climate data from CRU (such as described in additionally to any bias calculated for the mass balance calibration, see section 2.3). The results are then used as initial state for projection runs. For these, we used General Circulation Models (GCM) climate data originating from the CMIP6 (Eyring et al., 2016), which

employs Shared Socioeconomic Pathways (SSP) as scenario framework (Riahi et al., 2017). Since our objective is to assess the sensitivity of peak water to initial ice thickness rather than to provide precise climate projections, we restricted our analysis to a single GCM for computational efficiency. The choice to use only one GCM would be inaccurate if we were trying to assess accurately and precisely the future evolution of glaciers, but here we are solely interested in the study of the impact of different ice thickness datasets on glaciers and their runoff. We arbitrarily selected MRI-ESM2.0, which, out of an ensemble of 6 GCMs, locates itself below the average. More specifically, the GCM is the lowest of all, reaching 2°C and 5°C below the average in 2300 under the SSP1-2.6 and the SSP5-8.5 respectively. To account for climatic uncertainty, we further performed synthetic perturbations of the MRI climate by modifying mean temperature (see Section 2.6), which allows us to explore the influence of temperature bias on peak water timing and magnitude. While this approach cannot fully replace the use of a complete GCM ensemble—which would also capture evolving patterns of precipitation and seasonality—it nevertheless enables us to explore a broad range of artificial climatic conditions and their implications for peak water.

3 Results

3.1 Peak water sensitivity to initial volume and temperature

Figure 2 presents the sensitivity analysis of the peak water with respect to varying initial thicknesses and temperature bias under SSP1-2.6 and SSP5-8.5 (see section 2.6). It appears clearly that the smaller the Our results clearly indicate that a smaller initial ice volume of the glaciers, the earlier the peak water occurs, especially under the SSP5-8.5 leads to an earlier occurrence of peak water (Fig. 2a). Indeed, increasing the total ice volume will not significantly advance the timing of the peak water for Glacier runoff curves for SSP1-2.6 (~ 2060), hence suggesting it has not been reached under this climate forcings. On the contrary, multiplying .5 and SSP5-8.5 follow a similar trend, with the latter being 10 to 20 years above the first for the same initial ice volume. Under both scenarios, multiplying this volume by a factor of two under SSP5-8.5 will delay is delaying the timing of the peak water by roughly 25 years . Similarly, (e.g., reaching 2120 under SSP5-8.5). Similarly decreasing the initial ice volume by a factor 0.25, under the same scenario, will advance the timing of the of 0.1 will advance peak water by more than 90 years , from 2150 (multiplying factor of 1) to 2060 (Fig. 2a).

25 and 20 years for SSP1-2.6 and SSP5-8.5, respectively. The magnitude of annual runoff at peak water seems to follow a similar trend also increases with initial ice volume but trends differ more between scenarios (Fig. 2b): for SSP1-2.6 , it rises slightly from ~ 100 m^3 s^{-1} to ~ 125 m^3 s^{-1} going from a multiplying factor of 0.1 to reach a plateau from the coefficient 0.7 1.5, and then remains constant , at the level of 2300 Mt of water per year. For small coefficients, annual runoffs at peak water are quite close for both scenarios but then the magnitude of peak water under the at this level for higher initial ice volumes. Regarding SSP5-8.5 increases more rapidly: halving .5, runoff starts at 160 m^3 s^{-1} for a 0.1 factor and then constantly rises. Indeed, doubling the initial ice volume causes a decrease of 25 an increase of 45 % in annual runoff . Then, again, peak watermagnitude rises less when we are increasing ice volumeat peak water, reaching 380 m^3 s^{-1}.

Temperature bias seems to have little influence on Under SSP5-8.5 temperature bias linearly influences peak water timing under the SSP1-2.6 (Fig. 2c), however it has an impact on annual runoff at peak water: the latter grows perfectly linearly

along the range of bias(Fig. 2d). Indeed, a bias of 4: being in average advanced by 12.5 years for each 1°C induces a rise of 30 % in runoff. When it comes to the C increase in temperature bias. However, the magnitude of peak water does not change significantly with temperature bias, varying by roughly ± 10% compared to the magnitude without any temperature adjustment. This is not the case for the most optimistic scenario, where runoff at peak water linearly rises with positive temperature bias at a rate of 35 m^3 s^{-1} per added degree Celsius, reaching almost the same level as SSP5-8.5, peak water timing decreases almost linearly as temperature bias rises; a bias of +2.5 with a 5°C induces an advance of more than 15 yearsof the peak water. Even though annual runoff also increases with temperature bias, its curve is less steep than the one for the bias. Under SSP1-2.6: a bias of 4, adding a lower negative bias is delaying peak water by no more than 10 years, until there is a sudden increase between -3.5 and -5 °Conly results in a rise of 8 % of runoff.

Peak water sensitivity: peak water timing **(a)** and runoff at peak water **(b)** for different fractions of the initial ice volume, and peak water timing **(c)** and runoff at peak water **(d)** for different temperature bias. All of these simulations have been carried out using ice thickness data from Millan et al. (2022). Results are presented only for SSP-1.2.6 and SSP-5.8.5, since very little differences are visible between SSP1.2.6 and SSP5.3.4.

3.2 Future projection of evolution using existing ice thickness models

Figure 3 presents glacier simulations using the two global ice thickness estimates, in terms of ice volume, glacierized area, and annual runoff for the time period 2003-2300. We analyze the entire glacier region . Conversely, positive temperature bias almost linearly advances peak water timing, reaching the same year (i.e. 160 glaciers) by computing the cumulative evolution of the different variables2035) as SSP5-8.5 for a 5°C bias.

3.2 Future projections of evolution using existing ice thickness models

Monthly climate conditions provided by the model MRI-ESM2-0 (averaged over a 20-year window) in the region vary for the different glaciers of the set GCMs (Fig. 3c). Depending on the glacier, temperature can vary by almost 43d). The standard deviation of the GCM ensemble increases along the decades after 2050, especially under SSP5-8.5, reaching approximately 4.5°C and precipitations by nearly 5 kg. m^{-2} . Therefore, we used the mean of these variables to compare it with glacier evolution. The two forcing pathways used start differing around 2030 for temperature and around 2075 for 0.12 mm/d in 2300 for temperature and precipitation respectively. The forcing pathways start to notably differ around 2040 for mean temperature and precipitation. Regarding temperature, it slowly rises from lower than -9-6.5°C, further continues increasing until 2.5°C around 2215 2235 under the SSP5-8.5, and then stabilizes at 9°C. Under scenario SSP1-2.6, temperature maintains constant from 2050 at -7.5at -4.5°C and then decline throughout the decades and returns at an early 21st century level. for 2050 - 2100, declines until -5°C throughout the next 50 years and remains nearly steady until 2300. Precipitation rises from 6 kg m^{-2} 0.14 mm/d in 2015 to 12 kg m^{-2} 0.22 mm/d in 2300 for the SSP5-8.5. After a quick gain and loss an increase in the end of the 21st century, precipitation keeps constant from 2125 at nearly 7.5 kg.m^{-2} declines and then keeps roughly constant from 2165 a bit below 0.1 mm/d in SSP1-2.6. SSP5-3.4-OS mostly follows trends of SSP1-2.6 with a maximum deviation reaching 0.5°C and less than 0.02 mm/d in temperature and precipitation during the 2050-2120 period.

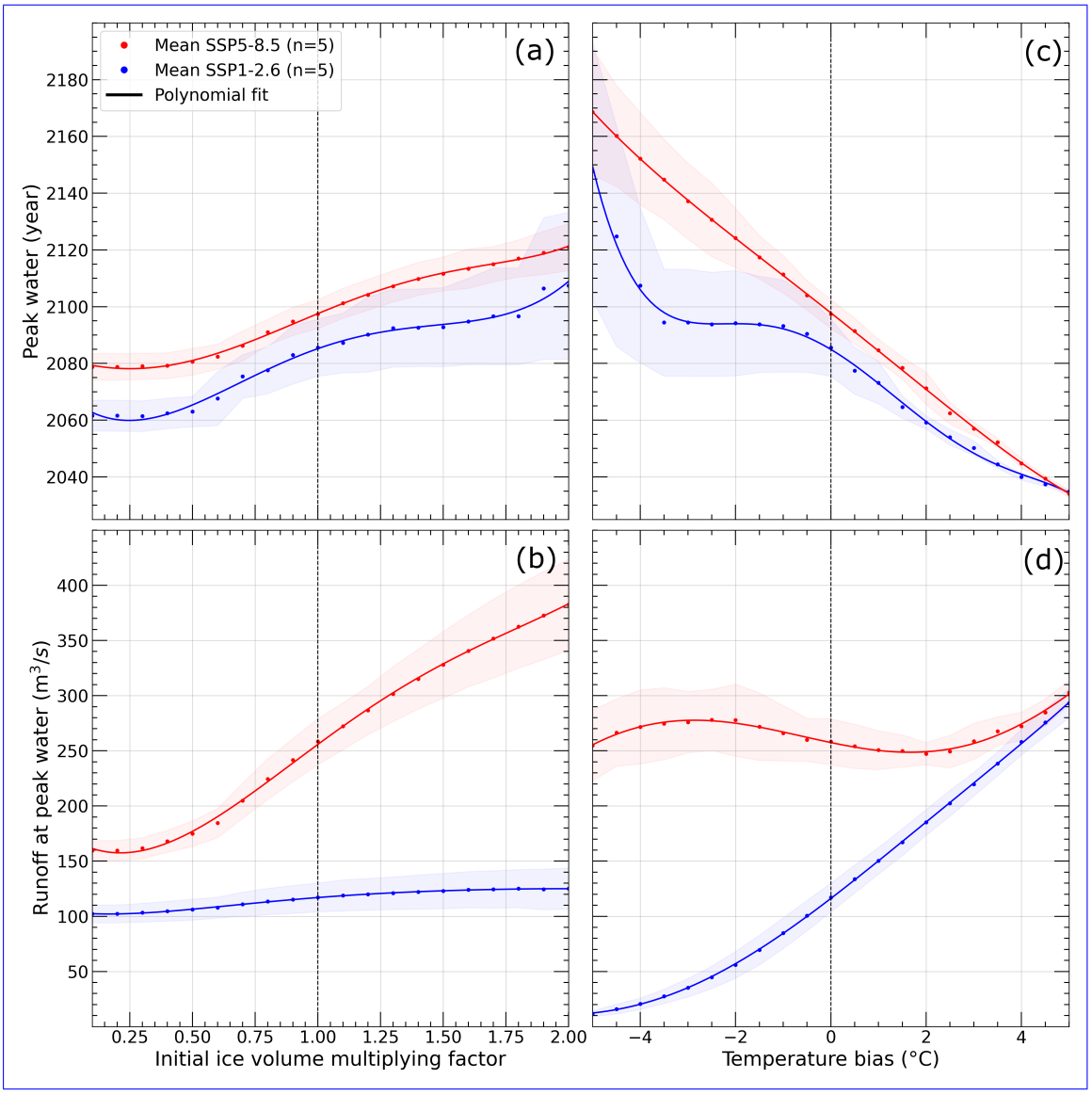

Figure 2. Timing and runoff at peak water for varying initial ice volume fractions **(a-b)** and temperature biases **(c-d)**. All of these simulations have been carried out using ice thickness data from MIL22. Results are presented only for SSP-1.2.6 and SSP-5.8.5 (few differences are visible between SSP1.2.6 and SSP5.3.4-OS) with multi-GCM mean shown in bold and shading indicating the mean ± 1 standard deviation of the GCM ensemble.

The significant differences between the two ice thickness datasets ~~translates~~ translate into an equally important one for glaciers ice volume loss ~~. At the beginning of the 21st century~~(Fig 3.a). After the dynamic spin-up and before future projections simulations, regional volume calculated from FARI19 (~~344~~ ~ 330 km^3) represents ~~roughly~~ 60 % of that computed from MIL22

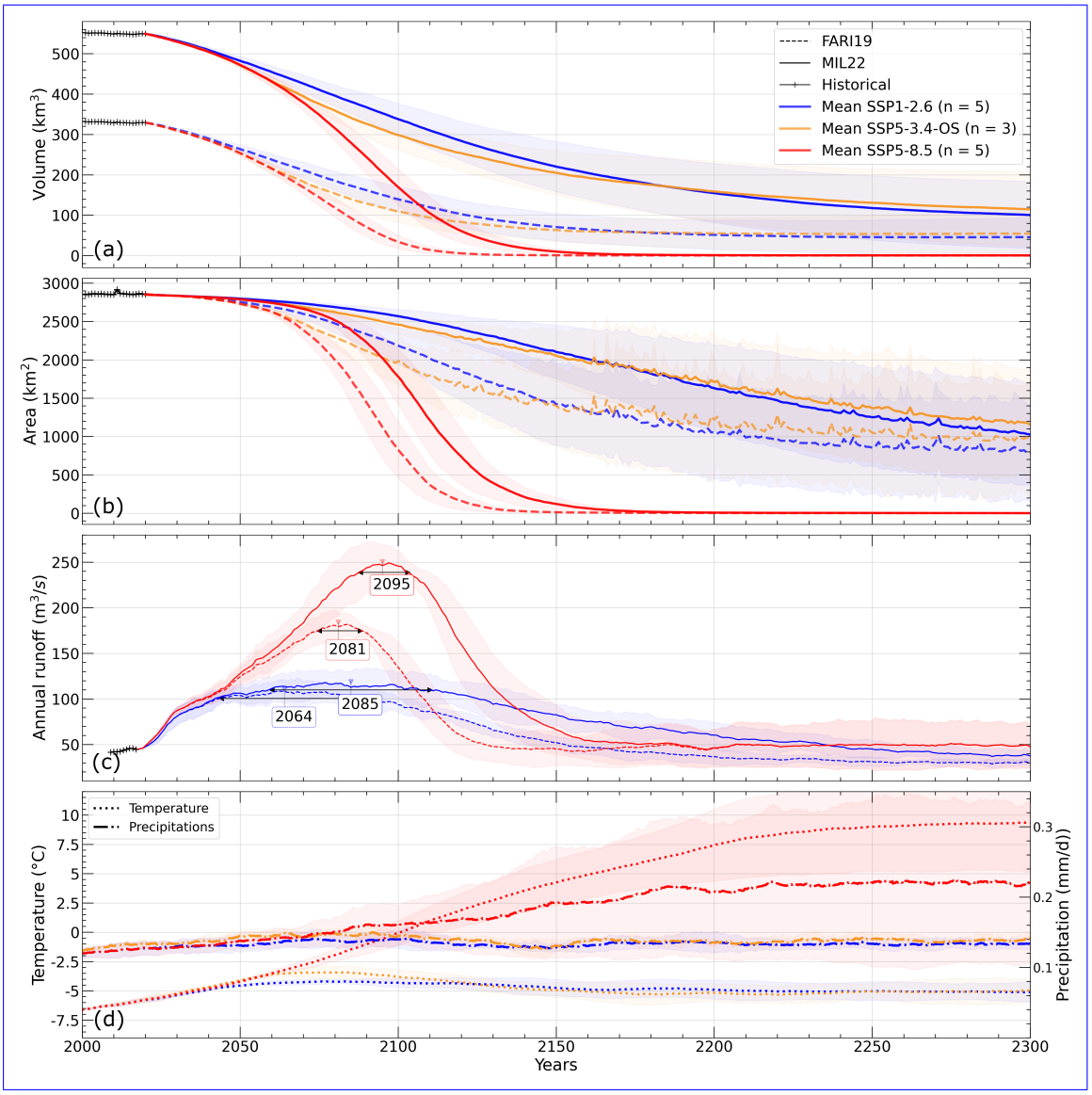

Figure 3. Projections of glacier evolution in the region of interest: the cumulative of all 160 glaciers **(a)** volumes, **(b)** areas and **(c)** annual runoffs, with an assessment of peak water timing, accompanied by **(d)** mean temperatures and precipitations projections under various SSPs (multi-GCM mean shown in bold, shading is the mean ±1 standard deviation of the GCM ensemble).

(~~562~~ ~ 550 km^3) (Fig. 3a). ~~Under the~~ We note that these ice volumes are lower than those computed in section 2.2, both by roughly 4%: this is a recognized weakness of OGGM's dynamical spin-up that glacier area and volume are not strictly the same at the glacier inventory date as after the inversion. Under SSP1-2.6~~and the SSP5-3.4~~, the total volume of ice equals ~~161~~ ~ 100 km^3 and ~~26~~ ~ 25 km^3 in 2300 for MIL22 and FARI19 respectively. This translates into a volume reduction of 92 % for

FARI19 and ~~71~~82% for MIL22. Under SSP5-8.5, the volumes declines at a higher rate ~~starting in 2070. In 2300, all the glaciers have almost completely disappeared, with an ice volume of 0.5~~ after 2040, so that very few ice volume is remaining from 2150 onwards (9 km ^{3} and ~~6~~ 0.7 km^3 for ~~FARI19 and~~ MIL22 ~~respectively.~~ and FARI19 respectively). For both datasets, less than 1 km^3 of ice persists at the end of the 23st century. Trajectories under SSP5-3.4-OS follow the ones forced with SSP5-8.5 until after 2060; then volumes change trends to reach and overtake the ones of SSP1-2.6 in 2175.

As glaciers lose mass, we can also see their surface area receding. The regional glacierized surface ~~areas (2872~~ area ($\sim$ 2850 km^2 at the beginning of simulations) ~~trend~~ slowly decreases until trends start to differ between ~~scenarios around 2050~~ climate scenarios around 2045 (Fig. 3b). The glacierized area of the consensus decreases at a faster rate than the one of ~~Millan for the two more optimistic SSPs~~ MIL22 for SSP1-2.6 with a loss of ~~21~~ $\sim$ 13 km^2.yr^{-1} against ~~8~~ $\sim$ 7 km^2.yr^{-1} in average for the ~~period~~ 2050-2150 time period. Hence, in 2300 ~~the consensus and the Millan~~ FARI19 and MIL22 areas have declined by ~~78 % and 45~~ 72 % and 63 % respectively. Curves based on the SSP 5-8.5 still stand out with a higher loss rate, ~~averaging 33~~ which is very similar for FARI19 and MIL22, averaging $\sim$ 27 km^2.yr^{-1} during 2040-2150, before most glaciers disappear completely. Indeed, while in 2150 there is still a total glacierized area equivalent to 114 km^2 and ~~17~~ 12 km^2 ~~. yr^{-1} in 2050-2150~~ ^{2} for ~~FARI19~~ MIL22 and ~~MIL2022 respectively. This leads to a reduced area of 6~~ FARI19 respectively, less than 2 km^2 ~~for the consensus ice thicknesses and 160 km^2 for the MIL2022 dataset, in 2300.~~ remain in 2300 for both datasets.

In response to such changes in ~~the~~ glaciers characteristics, ~~their hydrological outputs~~ glacier hydrological contributions are also modified along the decades. Here, we present simulated annual runoff ~~,~~ averaged over a ~~10-years~~ 10-year window for better readability (Fig. ~~3d~~3c); for the same reason~~we also didn't add~~ , we do not show simulations forced with ~~the~~ SSP5-3.4~~on the figure~~-OS on this figure, but they are included in Fig. S2. Runoff starts at the same level for the two datasets, ~~which is 1800 Mt of water per year, equivalent to a runoff of 57~~ being around 45 m^{3}s^{-1}, ~~because~~ since the initial glacier surface area is identical for all simulations. ~~It is worth mentioning that previous work (Gao et al., 2010) estimated average annual glacier runoff in the Tarim River Basin, using observations of annual discharge of mountain river runoff from hydrological stations along with temperature and precipitation monthly time series from national meteorological stations. For the period 1961-2006, the annual runoff was estimated to 144.16×10^8 m^3 , i.e., a runoff of 457 m^3 s^{-1} . The maximum of annual runoff calculated in this study (3400 Mt yr^{-1} , Fig. 3d) is roughly equal to a runoff of 108 m^3 s^{-1} . Hence, while the selected glaciers represent 24 % of the TIRB glacier ice volume (if we use volumes derived from MIL22), our runoff calculation seems to be realistic.~~

~~Under the~~ Under SSP1-2.6, after the first decades of simulation, FARI19 annual runoff goes from ~~1800 Mt to 2260 Mt in year 2056.~~ 45 m^3 s^{-1} to 105 m^3 s^{-1} in year 2064. The plateau around this ~~peak last approximately 45 years before glacier runoff softly diminishing~~ "peak" lasts approximately 40 years before glaciers runoff slowly diminishes until reaching a runoff of ~~less than 1000 Mt.yr~~30 m^3 s^{-1} in ~~2300.~~ 2250 and remaining constant for the last five decades of simulation. MIL22 runoff also rises from ~~1800 to 2300 Mt.yr~~45 to 115 m^3 s^{-1}, with a peak located in year ~~2064~~ 2085 and a plateau of ~~the same length~~50 years, and then declines during the following decades. In the year 2300, the runoff value is less than ~~1500 Mt.yr~~40 m^3 s^{-1}. Under ~~the~~ SSP5-3.4-OS, FARI19 annual runoff reaches peak water at 125 m^3 s^{-1} in 2061, while it is assessed at 135 m^3 s^{-1} in 2065 using MIL22. In both cases, runoff declines after a plateau lasting 25 to 30 years depending on the dataset, before going below runoff levels of SSP1-2.6 (Fig. S2). Under SSP5-8.5, annual runoff ~~increase steadily from 1800 Mt to~~ increases steadily

until reaching a peak of ~~2700 Mt in year 2108~~ 180 $m^3 s^{-1}$ in year 2081 for FARI19. For MIL22, ~~the~~ runoff increases to a peak of ~~3500 Mt in 2137 for MIL22.~~ almost 250 $m^3 s^{-1}$ in 2095. In both cases, the plateau lasts ~~roughly 60~~ between 10 to 15 years (Fig. ~~3d~~3c). Then, the two annual runoff curves decline with an offset in time, and an average runoff difference of ~~30~~∼ 40%. This ~~differences become smaller when they end up almost at same level as their respective SSP1-2.6 annual runoff values in year 2270. The~~ difference becomes smaller before fading away completely around 2190, when glaciers shrank so much that runoff is from now on almost entirely composed of snow melt and liquid precipitation on ice-free areas as indicates the evolution of annual runoff ~~with~~ decomposed by its four different contributions ~~is also available~~ (Fig. S1). The latter highlights that under SSP1-2.6 and after 2150, runoff is mostly sustained by snow melt of ice-free areas with FARI19, whereas ice melt on glacier remains the largest component with MIL22. Under SSP5-8.5 annual runoff is largely due to precipitation on ice-free areas with both datasets.

4 Discussion

4.1 Peak water dynamics and sensitivity

Our study reveals that the timing and magnitude of peak water are significantly influenced by the initial ice volume of ~~the~~ glaciers under certain conditions. This sensitivity underscores the importance of accurate ice thickness estimations to predict future water availability (Fig. 2). Contrasting responses observed between emissions scenarios highlight the non-linear influence of climate forcing on glacier runoff. The analysis reveals a particular sensitivity of the study region to the ice thickness model under the SSP5-8.5 scenario, which presents conditions sufficient for glaciers to reach a peak water tipping point and toward an ineluctable decrease of their contribution to river runoff~~(~~, unlike SSP-1.2.6 ~~where an "intermediate" peak in runoff seems to be reached). The difference~~ (see below). Differences in the initial ice volume also ~~has~~ have a significant influence on the magnitude of peak water (Fig. 2). As shown in Figures 2 and 3, a thicker glacier will at the same time provide more ice for runoff, but will also take longer to melt at lower elevations, keeping ice lower and more out of balance with the climate. This will translate into more negative surface mass balance rates, which in turn will produce increased runoff.

In the case of the SSP1-2.6 scenario, changes in the magnitude of peak water between the two datasets are not particularly significant (Fig. 2 and 3). This can be explained by the impact of the chosen climatic region for the simulations. Indeed, the projected climate under SSP1-2.6 is not warm enough to raise the equilibrium line to reach the conditions required for peak water. Thus, runoff evolution under the optimistic scenarios largely follows the temperature and precipitation trends, which in this case stabilizes after 2050 (Fig. 3d). Therefore, it is possible that in this specific case, peak water as a tipping point is never reached, and what we can see in the simulation results could more likely be identified as a melting peak, and the same applies to simulations conducted with SSP5-3.4 (Fig. S2). It is worth noting that the glacier volume and area continue to decrease during the entire time period, and that all results concern the average behavior of 160 different glaciers.

Within the temperature range explored in this study, it appears that peak water is more sensitive to temperature uncertainty than to differences in initial ice volume, in terms of peak water timing but also of peak water runoff under SSP1-2.6. The sudden increase in peak water timing under this scenario towards coldest bias is quite difficult to interpret and may be linked

to the method we use to measure peak water as a plateau: the climate is so cold that actually peak water is not occurring, runoff is remaining constant at a low level, and this is largely delaying what is assessed as the peak water year. It should also be taken into account that extremely cold temperature bias put some glaciers so out of balance with the climate that they grow outside the model domain boundaries and then cannot be simulated further, which will cause variations in the regional runoff when compared with a no bias situation. There are also non-negligible uncertainties regarding the GCMs used as climate forcing, especially concerning peak water timing: differences across GCMs can reach 80 and 40 years for SSP1-2.6 and SSP5-8.5, respectively.

Regarding runoff values obtained with future projections, it is worth noting that previous work (Gao et al., 2010) estimated average annual glacier runoff in the Tarim River Basin, using observations of annual discharge of mountain river runoff from hydrological stations along with temperature and precipitation monthly time series from national meteorological stations. For the 1961-2006 period, the annual runoff was estimated to 144.16×10^8 m^3 , i.e., a runoff of 457 m^3 s^{-1} . Maximum annual runoff calculated in this study (Fig. 3c) ranges from 105 m^3 s^{-1} with FARI19 to 115 m^3 s^{-1} with MIL22 under SSP1-26. Hence, while the selected glaciers represent 14 to 24 % of the TIRB glacier ice volume (if we use volumes derived from FARI19 or MIL22), our runoff calculations seem to be realistic.

It should also be mentioned that other sources of uncertainties subsist regarding the assessment of peak water other than those explored in the sensitivity tests, such as the calibration of the surface mass balance and ice flow dynamics models (Huss and Hock, 2015), as well as precipitation projections. Indeed, as shown in Figure 3d, precipitation standard deviation of the GCM ensemble is roughly equal to 50 % of the mean precipitation in 2300 under SSP5-8.5.

4.2 Influence of ice rheology on glacier dynamics and runoff

From a methodological point of view, we ~~choosed~~ chose to adjust the creep parameter A to match external ice thicknesses products, which introduces an intrinsic ambiguity: to obtain thicker ice in an inversion, A is often reduced. It is worth noting that a stiffer ice will ~~slows~~ slow down glacier flow, therefore delaying ice transport toward the ablation area. This has the potential to further postpone the timing of peak water, compounding the delay already induced by the larger total ice volume. Despite this rheological adjustment, we posit that the timing of peak water is primarily controlled by the initial ice volume and hypsometry. Under the ~~Shallow Ice Approximation~~SIA, ice flux through a cross section roughly scales as $q \sim Ah^5$ for Glen's flow law with exponent n=3 ~~(assuming~~ if assuming that slope is unchanged, and a rectangular cross section depending on the thickness ~~) Hutter (1983); Maussion et al. (2019)~~(Hutter, 1983; Maussion et al., 2019). Therefore, a simple scaling shows that changes in A affect the ice flux linearly, whereas variations in ice thickness have a much stronger, nonlinear impact on the flux. This suggests that initial geometry dominates the glacier response and sets the timing of peak water, while variations in A play a secondary role. Future work could explore ~~more quantitatively~~ the sensitivity of peak water to variations in ice rheology more quantitatively while keeping initial ice thicknesses fixed, in order to better isolate and understand the secondary influence of A on glacier runoff dynamics.

~~In the case of the SSP1-2.6 scenario, the changes in the timing of peak water between the two datasets are not particularly significant (Fig. 2 and 3). This can be explained by the impact of the chosen climatic region for the simulations. Indeed, the~~

projected climate under SSP1-2.6 is not sufficient to bring glaciers close to the geomorphological conditions required to reach peak water. Thus, runoff evolution under the optimistic scenarios largely follows the temperature and precipitation trends, which in this case stabilizes after 2050 (Fig. 3c). Therefore, it is possible that, in this specific case, peak water as a tipping point has not actually been reached, and what we observe could more likely be identified as a melting peak. It is worth noting that the glacier volume and area continued to decrease during the entire time period, and that all results concern the average behavior of 160 glaciers.

4.3 Uncertainties and limitations in ice thickness data

The contrasting responses observed between the SSP1-2.6 and SSP5-8.5 scenarios highlight the non-linear influence of temperature bias on glacier runoff and peak water timing. Under SSP1-2.6, although seasonal melting is sufficient to cause continued glacier mass loss, the timing of peak water remains largely unchanged, with only limited variation across the bias range. However, annual runoff at peak water increases almost linearly with temperature bias, suggesting that warming increases surface melt, but without significantly accelerating overall glacier losses. In contrast, under SSP5-8.5, increased temperature bias leads to a more pronounced shift in peak water timing. While runoff also increases with temperature bias, the relative change is smaller than under SSP1-2.6, likely due to the faster depletion of ice volume. This highlights how the influence of temperature uncertainty varies with climate scenario, likely affecting the timing of peak water more under high-emission pathways, and runoff magnitude more under low-emission ones.

Projections of glacier evolution in the region of interest: the cumulative of **(a)** all glacier volumes, of **(b)** glacier areas and of **(d)** annual runoffs of the glaciers of the set, with an assessment of peak water timing, accompanied by **(c)** the temperatures and precipitations projections from GCM MRI-ESM2.0. Time series used for each glaciers of the set are in light, and the respective means for SSPs 1-2.6 and 5-8.5 are in bold.

The improvement of global ice thickness models is a critical issue that depends on several factors. Ice thickness inversion models that rely on surface gradients are only using surface data that carries minimal information about glacier ice dynamics. The inclusion of ice surface velocities, and 2D inversions, introduces a strong constraint into glacier ice thickness inversions, which translates into a much realistic inverted ice thickness field (Millan et al., 2022; Cook et al., 2024). Flow Ice surface velocity measurements must therefore be continued over time to provide repeated measurements that can be synchronized with other data, such as Digital Elevation Models (DEMs)DEMs, surface mass balance or penetrating radar measurements (known limitations of the previous method). Future innovative satellite missions could certainly enable the mapping of glacial flow in three dimensions and synchronously with DEMs, which will provide significant advancements in estimating ice volumes, by reducing uncertainties on the temporal mismatch between satellite observations, and improving characterization of basal sliding and ice deformation Kääb et al. (2024).

Additionally, thickness estimates are highly dependent on the calibration of laws describing ice flow, particularly rheology (creep parameterand basal sliding)) and others processes such as basal sliding. To calibrate these laws, models use in-situ ice thickness measurements, the spatial scarcity of which leads to significant volume differences, as is the case with glaciers in the high mountains of Asia (Millan et al., 2022; Farinotti et al., 2019). Although advanced new approaches (Bolibar et al.,

2023; Cook et al., 2024; Jouvet, 2023) ~~will~~ can potentially better constrain these parameters, it is essential to obtain better spatial coverage of in-situ ice thickness in critical regions such as High Mountain Asia and the Andes. Synchronized planning of measurement campaigns with satellite missions is also crucial to minimize uncertainties related to temporal mismatches between observations, which are subsequently complex to quantify. ~~An open science policy for sharing existing (but unshared) observations, combined with a sufficient environmental approach — prioritizing only essential data collection and simulations — can both reduce model uncertainties and minimize research environmental impact while maximizing societal and scientific value.~~

4.4 Model limitations and implication for large-scale simulations

Finally, this study ~~highlights~~ shows the difficulty of accounting for the spatial distribution of ice thicknesses, derived from multi-source inversions, in large-scale glacier models. A major obstacle lies in the challenge of using 2D thickness inversions from external datasets as direct constraints in OGGM, which adjusts the bedrock depth to remain consistent with the simulated glacier dynamics. This critical aspect, which is key to the timing of future glacier evolution—and thus peak water—still remains to be explored. New approaches must be developed to incorporate multi-source thickness measurements as input constraints in large-scale models. New 2D or 3D models (Jouvet, 2023; Bolibar et al., 2023) have recently emerged and are therefore promising for ~~updating~~ better assimilating distributed observations to update this study. In a broader picture, this study highlights the importance of studying ~~models uncertainty for future glacier changes~~model uncertainty for glacier projections, especially the initial state of glaciers (Marzeion et al., 2020).

5 Conclusion

This study highlights the strong sensitivity of peak water timing and magnitude to uncertainties in initial glacier thickness and temperature biases in climate models. In regions where ice thicknesses are highly uncertain, such as the Western Kunlun mountains, peak water can be delayed by a decade, while its magnitude can change by up to 27% depending on the data source used under SSP-5.8.5. With the same scenario, peak water date can be brought forward by roughly a decade for each degree of temperature bias in the climate forcing data used. Finally, our results emphasize that accurate estimates of glacier geometry are crucial for robust projections of future water availability.

Code availability. The code to perform the simulations will be posted on a git-hub repository upon acceptance of the paper.

Data availability. All data used in this paper are freely available, and can be accessed at https://www.theia-land.fr/ces-cryosphere/glaciers/, https://www.research-collection.ethz.ch/handle/20.500.11850/315707 and through the OGGM shop https://docs.oggm.org/en/stable/shop.html.

Author contributions. LG, RM and NC conceived and designed the research. LG processed, analyzed data and performed all simulations. All authors participated in the writing of the manuscript.

Competing interests. We declare that we have no competing interests.

Acknowledgements. LG, NC, RM and JB acknowledge support from the Centre National de la Recherche Scientifique.

References

Aguayo, R., Maussion, F., Schuster, L., Schaefer, M., Caro, A., Schmitt, P., Mackay, J., Ultee, L., Leon-Muñoz, J., and Aguayo, M.: Assessing the glacier projection uncertainties in the Patagonian Andes (40–56° S) from a catchment perspective, EGUsphere, 2023, 1–41, https://doi.org/10.5194/egusphere-2023-2325, 2023.

Arias, P. A., Bellouin, N., Coppola, E., Jones, R. G., Krinner, G., Marotzke, J., Naik, V., Palmer, M. D., Plattner, G.-K., Rogelj, J., Rojas, M., Sillmann, J., Storelvmo, T., Thorne, P. W., Trewin, B., Achuta Rao, K., Adhikary, B., Allan, R. P., Armour, K., Bala, G., Barimalala, R., Berger, S., Canadell, J. G., Cassou, C., Cherchi, A., Collins, W., Collins, W. D., Connors, S. L., Corti, S., Cruz, F., Dentener, F. J., Dereczynski, C., Di Luca, A., Diongue Niang, A., Doblas-Reyes, F. J., Dosio, A., Douville, H., Engelbrecht, F., Eyring, V., Fischer, E., Forster, P., Fox-Kemper, B., Fuglestvedt, J. S., Fyfe, J. C., Gillett, N. P., Goldfarb, L., Gorodetskaya, I., Gutierrez, J. M., Hamdi, R., Hawkins, E., Hewitt, H. T., Hope, P., Islam, A. S., Jones, C., Kaufman, D. S., Kopp, R. E., Kosaka, Y., Kossin, J., Krakovska, S., Lee, J.-Y., Li, J., Mauritsen, T., Maycock, T. K., Meinshausen, M., Min, S.-K., Monteiro, P. M. S., Ngo-Duc, T., Otto, F., Pinto, I., Pirani, A., Raghavan, K., Ranasinghe, R., Ruane, A. C., Ruiz, L., Sallée, J.-B., Samset, B. H., Sathyendranath, S., Seneviratne, S. I., Sörensson, A. A., Szopa, S., Takayabu, I., Tréguier, A.-M., van den Hurk, B., Vautard, R., von Schuckmann, K., Zaehle, S., Zhang, X., and Zickfeld, K.: Technical Summary, pp. 33–144, Cambridge University Press, Cambridge, United Kingdom and New York, NY, USA, https://doi.org/10.1017/9781009157896.002, 2021.

Bolibar, J., Sapienza, F., Maussion, F., Lguensat, R., Wouters, B., and Pérez, F.: Universal differential equations for glacier ice flow modelling, Geoscientific Model Development, 16, 6671–6687, https://doi.org/10.5194/gmd-16-6671-2023, 2023.

Brun, F., Berthier, E., Wagnon, P., Kääb, A., and Treichler, D.: A spatially resolved estimate of High Mountain Asia glacier mass, Nature Geoscience, 10, 668–673, https://doi.org/10.1038/ngeo2999, 2017.

Caro, A., Condom, T., Rabatel, A., and Champollion, N.: Future glacio-hydrological changes in the Andes: a focus on near-future projections up to 2050., Scientific Reports, 15, https://doi.org/10.1038/s41598-025-88069-2, 2025.

Cook, S., Jouvet, G., Millan, R., Rabatel, A., Maussion, F., Zekollari, H., and Dussaillant, I.: Global ice-thickness inversion using a deep-learning-aided 3D ice-flow model with data assimilation, EGU General Assembly Conference Abstracts, https://doi.org/10.5194/egusphere-egu24-8944, 2024.

Eyring, V., Bony, S., Meehl, G. A., Senior, C. A., Stevens, B., Stouffer, R. J., and Taylor, K. E.: Overview of the Coupled Model Intercomparison Project Phase 6 (CMIP6) experimental design and organization, Geoscientific Model Development, 9, 1937–1958, https://doi.org/10.5194/gmd-9-1937-2016, 2016.

Farinotti, D., Brinkerhoff, D. J., Clarke, G. K. C., Fürst, J. J., Frey, H., Gantayat, P., and Gillet-Chaulet, F.: How accurate are estimates of glacier ice thickness? Results from ITMIX, the Ice Thickness Models Intercomparison eXperiment, The Cryosphere, 11, 949–970, https://doi.org/10.5194/tc-11-949-2017, 2017.

Farinotti, D., Huss, M., Fürst, J., Landmann, J., Machguth, H., Maussion, F., and Pandit, A.: A consensus estimate for the ice thickness distribution of all glaciers on Earth, Nature Geoscience, 12, 168–173, https://doi.org/10.1038/s41561-019-0300-3, 2019.

Frank, T. and van Pelt, W. J. J.: Ice volume and thickness of all Scandinavian glaciers and ice caps, Journal of Glaciology, 70, https://doi.org/10.1017/jog.2024.25, 2024.

Fürst, J. J., Gillet-Chaulet, F., Benham, T. J., Dowdeswell, J. A., Grabiec, M., Navarro, F., Pettersson, R., Moholdt, G., Nuth, C., Sass, B., Aas, K., Fettweis, X., Lang, C., Seehaus, T., and Braun, M.: Application of a two-step approach for mapping ice thickness to various glacier types on Svalbard, The Cryosphere, 11, 2003–2032, https://doi.org/10.5194/tc-11-2003-2017, 2017.

Gagliardini, O., Zwinger, T., Gillet-Chaulet, F., Durand, G., Favier, L., de Fleurian, B., Greve, R., Malinen, M., Martín, C., Råback, P., Ruokolainen, J., Sacchettini, M., Schäfer, M., Seddik, H., and Thies, J.: Capabilities and performance of Elmer/Ice, a new-generation ice sheet model, Geoscientific Model Development, 6, 1299–1318, https://doi.org/10.5194/gmd-6-1299-2013, 2013.

Gao, X., Ye, B., Zhang, S., Qhiao, C., and Zhang, X.: Glacier runoff variation and its influence on river runoff during 1961–2006 in the Tarim River Basin, China, Science China Earth Sciences, 53, 880–891, https://doi.org/10.1007/s11430-010-0073-4, 2010.

Harris, I., Jones, P. D., Osborn, T. J., and Lister, D. H.: Version 4 of the CRU TS monthly high-resolution gridded multivariate climate dataset, Scientific Data, 7, https://doi.org/10.1038/s41597-020-0453-3, 2020.

Hersbach, H., Bell, B., Berrisford, P., Biavati, G., Horányi, A., Muñoz Sabater, J., Nicolas, J., Peubey, C., Radu, R., Rozum, I., Schepers, D., Simmons, A., Soci, C., Dee, D., and Thépaut, J.-N.: ERA5 monthly averaged data on single levels from 1979 to present, Copernicus Climate Change Service (C3S) Climate Data Store (CDS), https://doi.org/10.24381/cds.f17050d7, 2019.

Hock, R., Rasul, G., Adler, C., Cáceres, B., Gruber, S., Hirabayashi, Y., Jackson, M., Kääb, A., Kang, S., Kutuzov, S., Milner, A., Molau, U., Morin, S., Orlove, B., and Steltzer, H.: High Mountain Area, in: IPCC Special Report on the Ocean and Cryosphere in a Changing Climate, edited by Pörtner, H.-O., Roberts, D., Masson-Delmotte, V., Zhai, P., Tignor, M., Poloczanska, E., Mintenbeck, K., Alegría, A., Nicolai, M., Okem, A., Petzold, J., Rama, B., and Weyer, N., 2019a.

Hock, R., Rasul, G., Adler, C., Cáceres, B., Gruber, S., Hirabayashi, Y., Jackson, M., Kääb, A., Kang, S., Kutuzov, S., Milner, A., Molau, U., Morin, S., Orlove, B., and Steltzer, H.: High Mountain Areas, IPCC Special Report on the Ocean and Cryosphere in a Changing Climate, https://doi.org/10.5194/tc-14-565-2020, 2019b.

Hock, R., Maussion, F., Marzeion, B., and Nowicki, S.: What is the global glacier ice volume outside the ice sheets?, Journal of Glaciology, 69, 204–210, https://doi.org/10.1017/jog.2023.1, 2023.

Hugonnet, R., McNabb, R., Berthier, E., Menounos, B., Nuth, C., Girod, L., Farinotti, D., Huss, M., Dussaillant, I., Brun, F., and Kääb, A.: Accelerated global glacier mass loss in the early twenty-first century, Nature, 592, 726–731, https://doi.org/10.1038/s41586-021-03436-z, 2021.

Huss, M. and Farinotti, D.: Distributed ice thickness and volume of all glaciers around the globe, Journal of Geophysical Research: Earth Surface, 117, https://doi.org/10.1029/2012jf002523, 2012.

Huss, M. and Hock, R.: A new model for global glacier change and sea-level rise, Frontiers in Earth Science, 3, 54, https://doi.org/10.3389/feart.2015.00054, 2015.

Huss, M. and Hock, R.: Global-scale hydrological response to future glacier mass loss, Nature Climate Change, 8, 135–140, https://doi.org/10.1038/s41558-017-0049-x, 2018.

Hutter, K.: Theoretical Glaciology: Material Science of Ice and the Mechanics of Glaciers and Ice Sheets, D. Reidel Publishing Company, Dordrecht, Boston, Lancaster, Tokyo, https://doi.org/10.3189/S0022143000006055, 1983.

Immerzeel, W. W., Lutz, A. F., Andrade, M., Bahl, A., Biemans, H., Bolch, T., Hyde, S., Brumby, S., and Davies, B. J.: Importance and vulnerability of the world's water towers, Nature, 577, 364–369, https://doi.org/10.1038/s41586-019-1822-y, 2020.

Jouvet, G.: Inversion of a Stokes glacier flow model emulated by deep learning, Journal of Glaciology, 69, 13–26, https://doi.org/10.1017/jog.2022.41, 2023.

Ke, L., Ding, X., and Song, C.: Heterogeneous changes of glaciers over the western Kunlun Mountains based on ICESat and Landsat-8 derived glacier inventory, Remote Sensing of Environment, 168, 213–223, https://doi.org/10.1016/j.rse.2015.06.019, 2015.

Kienholz, C., Rich, J. L., Arendt, A. A., and Hock, R.: A new method for deriving glacier centerlines applied to glaciers in Alaska and northwest Canada, The Cryosphere, 8, 503–509, https://doi.org/10.5194/tc-8-503-2014, 2014.

Kääb, A., Mouginot, J., Prats-Iraola, P., Rignot, E., Rabus, B., Benedikter, A., Rott, H., Nagler, T., Rommen, B., and Lopez-Dekker, P.: Potential of the Bi-Static SAR Satellite Companion Mission Harmony for Land-Ice Observations, Remote Sensing, 16, https://doi.org/10.3390/rs16162918, 2024.

Körner, C., Jetz, W., Paulsen, J., Payne, D., Rudmann-Maurer, K., and Spehn, M.: A global inventory of mountains for bio-geographical applications, Alpine Botany, 127, 1–15, https://doi.org/10.1007/s00035-016-0182-6, 2017.

Lange, S., Menz, C., Gleixner, S., Cucchi, M., Weedon, G. P., Amici, A., Bellouin, N., Schmied, H. M., Hersbach, H., Buontempo, C., and Cagnazzo, C.: WFDE5 over land merged with ERA5 over the ocean (W5E5 v2.0), https://doi.org/10.48364/ISIMIP.342217, 2021.

Larour, E., Seroussi, H., Morlighem, M., and Rignot, E.: Continental scale, high order, high spatial resolution, ice sheet modeling using the Ice Sheet System Model (ISSM), Journal of Geophysical Research: Earth Surface, 117, https://doi.org/10.1029/2011jf002140, 2012.

Lee, J.-Y., Marotzke, J., Bala, G., Cao, L., Corti, S., Dunne, J. P., Engelbrecht, F., Fischer, E., Fyfe, J. C., Jones, C., Maycock, A., Mutemi, J., Ndiaye, O., Panickal, S., and Zhou, T.: Future Global Climate: Scenario-Based Projections and Near-Term Information, in: Climate Change 2021: The Physical Science Basis. Contribution of Working Group I to the Sixth Assessment Report of the Intergovernmental Panel on Climate Change, edited by Masson-Delmotte, V., Zhai, P., Pirani, A., Connors, S. L., Péan, C., Berger, S., Caud, N., Chen, Y., Goldfarb, L., Gomis, M. I., Huang, M., Leitzell, K., Lonnoy, E., Matthews, J. B. R., Maycock, T. K., Waterfield, T., Yelekçi, O., Yu, R., and Zhou, B., pp. 553–672, Cambridge University Press, Cambridge, United Kingdom and New York, NY, USA, https://doi.org/10.1017/9781009157896.006, 2021.

Lehner, B., Verdin, K., and Jarvis, A.: New Global Hydrography Derived From Spaceborne Elevation Data, Eos, Transactions American Geophysical Union, 89, 93–94, https://doi.org/10.1029/2008eo100001, 2008.

Linsbauer, A., Paul, F., and Haeberli, W.: Modeling glacier thickness distribution and bed topography over entire mountain ranges with GlabTop: Application of a fast and robust approach, Journal of Geophysical Research: Earth Surface, 117, https://doi.org/10.1029/2011JF002313, 2012.

Marzeion, B., Jarosch, A. H., and Hofer, M.: Past and future sea-level change from the surface mass balance of glaciers, The Cryosphere, 6, 1295–1322, https://doi.org/10.5194/tc-6-1295-2012, 2012.

Marzeion, B., Kaser, G., Maussion, F., and Champollion, N.: Limited influence of climate change mitigation on short-term glacier mass loss, Nature Climate Change, 8, 305–308, https://doi.org/10.1038/s41558-018-0093-1, 2018.

Marzeion, B., Hock, R., Anderson, B., Bliss, A., Champollion, N., Fujita, K., Huss, M., Immerzeel, W. W., Kraaijenbrink, P., Malles, J.-H., Maussion, F., Radić, V., Rounce, D. R., Sakai, A., Shannon, S., van de Wal, R., and Zekollari, H.: Partitioning the Uncertainty of Ensemble Projections of Global Glacier Mass Change, Earth's Future, 8, https://doi.org/10.1029/2019EF001470, 2020.

Maussion, F., Butenko, A., Champollion, N., Dusch, M., Eis, J., Fourteau, K., Gregor, P., Jarosch, A. H., Landmann, J., Oesterle, F., Recinos, B., Rothenpieler, T., Vlug, A., Wild, C. T., and Marzeion, B.: Open Global Glacier Model (OGGM) v1.1, Geoscientific Model Development, 12, 909–931, https://doi.org/10.5194/gmd-12-909-2019, 2019.

Millan, R., Mouginot, J., Rabatel, A., and Morlighem, M.: Ice velocity and thickness of the world's glaciers, Nature Geoscience, 15, 124–129, https://doi.org/10.1038/s41561-021-00885-z, 2022.

Nauels, A., Meinshausen, M., Mengel, M., Lorbacher, K., and Wigley, T. M. L.: Sea level projections to AD2500 with a new generation of climate change scenarios, Environmental Research Letters, 12, 114 002, 2017.

RGI Consortium, G.: Randolph Glacier Inventory – A Dataset of Global Glacier Outlines: Version 6.0 (Technical Report, Global Land Ice Measurements from Space, Colorado, USA), Tech. rep., https://doi.org/10.7265/N5-RGI-60, 2017.

Riahi, K., van Vuuren, D. P., Kriegler, E., Edmonds, J., O'Neill, B. C., Fujimori, S., Bauer, N., Calvin, K., Dellink, R., Fricko, O., Lutz, W., Popp, A., Cuaresma, J. C., Kc, S., Leimbach, M., Jiang, L., Kram, T., Rao, S., Emmerling, J., Ebi, K., Hasegawa, T., Havlik, P., Humpenöder, F., Da Silva, L. A., Smith, S., Stehfest, E., Bosetti, V., Eom, J., Gernaat, D., Masui, T., Rogelj, J., Strefler, J., Drouet, L., Krey, V., Luderer, G., Harmsen, M., Takahashi, K., Baumstark, L., Doelman, J. C., Kainuma, M., Klimont, Z., Marangoni, G., Lotze-Campen, H., Obersteiner, M., Tabeau, A., and Tavoni, M.: The Shared Socioeconomic Pathways and their energy, land use, and greenhouse gas emissions implications: An overview, Global Environmental Change, 42, 153–168, https://doi.org/10.1016/j.gloenvcha.2016.05.009, 2017.

Rounce, D. R., Hock, R., Maussion, F., Hugonnet, R., Radić, V., Bliss, A., de Vaan, G., Giesen, R. H., Goelzer, H., Huss, M., Immerzeel, W. W., Marzeion, B., Malles, J.-H., Pelto, B. M., Rastner, P., Rignot, E., Sakai, A., Shannon, S., van de Wal, R. S. W., and Zekollari, H.: Global glacier change in the 21st century: Every increase in temperature matters, Science, 379, 78–83, https://doi.org/10.1126/science.abo1324, 2023.

Sinergise Solutions d.o.o., &. P. L. c.: Sentinel Hub, https://www.sentinel-hub.com, accessed: 2025-10-02.

Taylor, K. E., Stouffer, R. J., and Meehl, G. A.: An Overview of CMIP5 and the Experiment Design, Bulletin of the American Meteorological Society, 93, 485–492, https://doi.org/10.1175/BAMS-D-11-00094.1, 2012.

Wester, P., Mishra, A., Mukherji, A., and Shrestha, A. B., eds.: The Hindu Kush Himalaya Assessment: Mountains, Climate Change, Sustainability and People, Springer International Publishing, Cham, ISBN 978-3-319-92287-4 978-3-319-92288-1, https://doi.org/10.1007/978-3-319-92288-1, 2019.

WGMS: Glacier Thickness Database 2.0, Tech. rep., https://doi.org/10.5904/wgms-glathida-2016-07, 2016.

WGMS: Fluctuations of Glaciers Database, World Glacier Monitoring Service, Zurich, Switzerland, https://doi.org/10.5904/wgms-fog-2021-05, 2021.

Yasuda, T. and Furuya, M.: Short-term glacier velocity changes at West Kunlun Shan, Northwest Tibet, detected by Synthetic Aperture Radar data, Remote Sensing of Environment, 128, 87–106, https://doi.org/10.1016/j.rse.2012.09.021, 2013.

Zekollari, H., Huss, M., Farinotti, D., and Lhermitte, S.: Ice-Dynamical Glacier Evolution Modeling—A Review, Reviews of Geophysics, 60, https://doi.org/10.1029/2021RG000754, 2022.

Zekollari, H., Huss, M., Schuster, L., Maussion, F., Rounce, D. R., Aguayo, R., Champollion, N., Compagno, L., Hugonnet, R., Marzeion, B., Mojtabavi, S., and Farinotti, D.: Twenty-first century global glacier evolution under CMIP6 scenarios and the role of glacier-specific observations, The Cryosphere, 18, 5045–5066, https://doi.org/0.5194/tc-18-5045-2024, 2024.